ACS OMEGA

http://pubs.acs.org/journal/acsodf

Article

# Ultrasonic De-cross-linking of the pH- and Magneto-Responsive PHEMA/PMMA Microgel to Janus Nanoparticles: A New Synthesis Based on "Grafting from"/"Grafting to" Polymerization

Rahim Ghanbarinia Firozjah, Amirhossein Sadeghi, and Sepideh Khoee*

Cite This: *ACS Omega* 2020, 5, 27119−27132

Read Online

ACCESS | Metrics & More | Article Recommendations | Supporting Information

**ABSTRACT:** Stimuli-responsive Janus nanoparticles (NPs) with a two-facial structure have been used widely in biomedical applications. Among several methods to prepare these NPs, surface-initiated atom transfer radical polymerization (SI-ATRP) has received much attention due to the precise deposition of polymers on the surface of the substrate. In this study, Janus nanoparticles with asymmetric surface chemistry were prepared through a masking method in three steps involving the covalent deposition of super paramagnetic iron oxide nanoparticles (SPIONs) on the cross-linked substrate based on methotrexate (MTX)-grafted poly(2-hydroxyethyl methacrylate) (CPM), surface functionalization of unreacted sites of immobilized SPIONs with 2-bromoisobutyryl bromide (BIBB) in order to prepare the macro-initiator (Br-$Fe_3O_4$-CPM), growing poly(methyl methacrylate) (PMMA) on the surface of the macro-initiator through the SI-ATRP method. Optical microscopy was utilized to monitor the successful modification of SPIONs. Poly(methyl methacrylate)-iron oxide-poly(2-hydroxyethyl methacrylate) (PMMA-$Fe_3O_4$-PHEMA) microgel was exposed to optimum ultrasound (US) waves to prepare the PMMA-$Fe_3O_4$-PHEMA nanoparticle. Transmission electron microscopy (TEM) was used to confirm the precise deposition of polymers and the Janus structure. The MTX release of US-synthesized Janus NPs was studied in PBS at pH values of 7.4 and 5.8. The release data were analyzed using the Excel add-in DDSolver program to evaluate the kinetics of the drug release process from the nanocarrier under different pH values.

## INTRODUCTION

Nanomaterials with different sizes, shapes, and chemical compositions, including metal and metal oxide nanoparticles (NPs), polymeric micelles, liposomes, carbon nanotubes, and carbon nanohorns, have been applied as nanocarriers for the delivery of therapeutic agents.[1,2] Among these nanosized particles, superparamagnetic iron oxide nanoparticles (SPIONs) with strong magnetic characteristic, suitable surface chemistry, and low toxicity have received noticeable attention as the contrast enhancement for magnetic resonance imaging (MRI),[3] therapeutic agents for tissue specific drug release,[4] and a component in tissue engineering.[5] However, the stability of SPOIN suspensions at physiological media and immunological stealthiness must receive great attention in order to use them for biomedical applications. Although SPOINs demonstrated low toxicity for *in vivo* application, these NPs are willing to agglomerate in a biological environment after salt and protein adsorption. Therefore, SPOINs can be modified through non-immunogenic biocompatible polymers to improve their stability, minimize the remnant magnetization, and prevent their agglomeration.[6] Poly(2-hydroxyethyl methacrylate) (PHEMA) as a stimuli-responsive polymer has been widely used in biomedical application. Armes et al. reported that HEMA-based homopolymers with low DP are completely water soluble instead of being merely water swellable. In addition, HEMA homopolymers with DP between 20 and 35 showed thermo-responsive behavior with cloud points changing from 28 to 39 °C at pH 6.5.[7] Poly(methyl methacrylate) (PMMA) is another biocompatible polymer that has been widely applied in biomedical applications after the first use on the development of nanoparticles for vaccination purposes by Kreuter et al.[8] Although its application as a drug particulate carrier system has been somehow limited due to its bio-inert and non-biodegradable properties, current reports have indicated a growing interest in its applications as a particulate carrier in drug delivery.[9] Surface modification of nanoparticles with two or more types of components, which have their own fingerprint optical, magnetic, and electronic properties, results in a Janus structure. Thus, these structures make it possible to use two different types of chemistry on one particle. Furthermore, due to asymmetrical functionalization, Janus nanoparticles have attained considerable attention in many fields such as surfactants, imaging nanoprobes, catalysts, self-motile colloidal materials, optical sensors, and therapeutic delivery systems. Masking, phase separation, and self-assembly are three ways of preparing Janus NPs. In the masking method, one side of primary particles is protected, whereas the other side of particles is available for functionalization. The phase-separation method is based on using incompatible components following their separation in their own patch. The self-assembly procedure is done by spontaneous self-assembly of

**Received:** June 9, 2020
**Accepted:** October 2, 2020
**Published:** October 14, 2020





https://dx.doi.org/10.1021/acsomega.0c02710
*ACS Omega* 2020, 5, 27119−27132

materials in an amphiphilic polymer. Among all mentioned procedures, the masking method has received much attention for preparing Janus particles.[10−15]

Stimuli-responsive Janus NPs have been prepared from biomaterials, which indicate direct and rapid responses to external signals such as temperature, pH, light, magnetic field, and ultrasound (US).[16] The US technique has been used in different areas such as engineering and medicine. The US penetrates through any substance and impacts on numerous properties of materials. Low-frequency US shows effectiveness with common applications. By way of an example, it is mainly used to dissolve substances or to homogenize mixtures. It has also gained popularity for use in many operations such as degasification and reducing particle size.[17,18] The US waves can be served as an external stimulus in copolymer microgels containing *N*-isopropylacrylamide (NIPAm) and acrylic acid (AA) using methylenebisacrylamide as a cross-linker. The US-triggered spherically polymeric microgels leaded to a change in hydrodynamic diameter in a water medium and volume phase-transition temperature of the microgels.[19] Moreover, US waves can be useful to trigger drug release and visualize the target during the therapeutic action through degradation of polymeric carriers.[20] Husseini et al.[21] showed that lower ultrasound frequencies (20 kHz) led to the highest levels of release of the anti-cancer agent doxorubicin (DOX), and the efficiency of drug release dwindled when the frequency enhanced up to 90 kHz. Similar results were achieved using pluronic micelles stabilized by an interpenetrating network of poly(*N*,*N*-diethylacrylamide) that prevented destabilization upon dilution.[22] Recent advance has also been made by exploring new ultrasound-cleavable micelle compositions and structures. Wang et al.[23] used a novel poly(ethylene oxide)-*block*-poly(2-tetrahydropyranyl methacrylate) (PEO-*b*-PTHPMA) copolymer to form ultrasound-responsive micelles with weaker chemical bonds in order to be more sensitive to both pH and temperature. The thermo-sensitivity of the mentioned copolymer was previously studied by Pelletier et al.[24] who showed that PEO-*b*-PTHPMA micelles are disrupted as a result of thermal hydrolysis of the 2-tetrahydropyranyl methacrylate (THPMA) side chains, converting to poly(methacrylic acid) PMAA and increasing the polarity and hydrophilicity of the polymer. Wang et al.[23] utilized the same micelle formulation to show that disruption of the side chains would be achievable with higher frequency ultrasound exposure (1.1 MHz).

Generally, physical adsorption of the polymer and covalent attachment by chemical reaction are two basic ways to deposit polymer brushes on the solid surface. A covalently bonded polymer could prevail over drawbacks that appeared by physical adsorption, like low grafting densities and adhesive force. "Grafting to" and "grafting from" approaches account for the most common procedures to covalently attach polymer brushes at a surface. In the "grafting from" approach, surface-initiated atom transfer radical polymerization (SI-ATRP) has reached much consideration due to its controlled/living characteristic, tolerance of functional groups, and high grafting density. Recently, Liu et al. prepared the Janus-like poly(methyl methacrylate)-*b*-poly(ethylene glycol)-folic acid *block*-copolymer-grafted fluorescent carbon dots (CDs-PMMA-PEG-FA) via surface-initiated atom transfer radical polymerization (SI-ATRP) of methyl methacrylate (MMA) in ethanol and used the modified carbon dots (CDs-Br) as an initiator followed by the PEGylation via click chemistry.[25]

In this work, we synthesized US-triggered Janus nanoparticles based on SPIONs modified with hydrophilic poly(2-hydroxyethyl methacrylate) (PHEMA) and hydrophobic poly(methyl methacrylate) (PMMA). Our strategy to prepare these nanocarriers is based on "grafting to" and "grafting from" approaches. Thus, methotrexate (MTX)-grafted low-molecular-weight PHEMA was first cross-linked through *Nα,Nα′*-di-Boc-L-cystine (Boc-Cys-OH)$_2$ in order to prepare a suitable substrate for covalent immobilization of modified SPIONs. To prepare Janus NPs, MMA monomers were grafted from unreacted sides of immobilized iron oxide nanoparticles through the SI-ARTP method before exposing the (PMMA-$Fe_3O_4$-PHEMA) microparticles to US waves. The MTX release behavior from Janus nanoparticles was studied at two different pH values of 7.4 and 5.8. Finally, in order to evaluate the kinetics of the drug release process from the nanocarrier under different pH values, the release data were analyzed using the Excel add-in DDSolver program.

## EXPERIMENTAL SECTION

**Materials.** Ethanolamine (EA), 2-bromoisobutyryl bromide (BIBB), triethylamine (TEA), *N*,*N*-dicyclohexylcarbodiimide (DCC), 4-dimethylaminopyridine (DMAP), copper bromide (CuBr), 2-hydroxyethyl methacrylate (HEMA), methyl methacrylate (MMA), di-*tert*-butyl dicarbonate ($BOC_2O$), dimethylformamide (DMF), dimethyl sulfoxide (DMSO), dichloromethane (DCM), toluene, 1,2-dichloroethane, hydrochloric acid (HCl), and tetrahydrofuran (THF) were all purchased from Merck Chemical Co. Moreover, *N*-hydroxysuccinimide (NHS), *N*-ethylcarbodiimide hydrochloride (EDC), 2,2′-bipyridine (bpy), succinic anhydride, *N*,*N*,*N*′,*N*″, *N*″-pentamethyldiethylenetriamine (PMDETA), methotrexate (MTX), *N*-(2-aminoethyl)-3-aminopropyltrimethoxysilane (APTES), ethyl α-bromoisobutyrate (EBIB), $FeCl_3{\cdot}6H_2O$, and $FeCl_2{\cdot}4H_2O$ were all purchased from Aldrich. All the chemicals were of analytical grade and used without any purification.

**Synthesis of the Methotrexate-Conjugated PHEMA (PHEMA-MTX) Microgel.** *Synthesis of PHEMA.* According to the reference,[26] PHEMA was prepared via atom transfer radical polymerization (ATRP), and EA-IBB was used as the ATRP initiator (Supporting Information). First, HEMA (4.78 g, 36.72 mmol) and CuBr (118.1 mg, 1.19 mmol) were dissolved in isopropanol (3.5 mL, 45.8 mmol) at room temperature. While the solution was being purged with nitrogen gas, the initiator (265 mg, 1.26 mmol) and 2,2′-bipyridine (0.46 g, 2.95 mmol) were separately dissolved in 0.5 mL of isopropanol and purged with nitrogen gas and then poured into the solution with a syringe. The mixture was stirred for 1 h under a nitrogen atmosphere. In order to quench the polymerization, the dark brown mixture was exposed to the air so that a blue color appeared completely well. Then, 4 mL of THF was added to the mixture, and the final solution was filtered over alumina to remove the catalyst. Next, the solvent was removed by vacuum evaporation. PHEMA was obtained as a white precipitate and then dissolved in methanol and precipitated in diethyl ether. This cycle was repeated three times to achieve a pure product.

*Conjugation of Methotrexate to PHEMA (PHEMA-MTX).* MTX (150 mg, 0.33 mmol), DCC (72 mg, 0.34 mmol), and NHS (40 mg, 0.34 mmol) were dissolved in DMSO (5 mL), and the solution was stirred for 1 h under nitrogen gas. Then, a solution of PHEMA (1 g, 0.21 mmol) and TEA (0.5 mL, 3.5 mmol) in DMSO (25 mL) was added to the mixture. While the final solution was being purged with nitrogen gas, it was


https://dx.doi.org/10.1021/acsomega.0c02710
ACS Omega 2020, 5, 27119−27132

stirred for 48 h. At the end, the white precipitate was removed by filtration, and the filtrate was freeze dried. To remove the redundant materials, the product was dissolved once in methanol and precipitated in diethyl ether and then in DMSO (solvent) and precipitated in water (non-solvent).

*Synthesis of Cross-linked PHEMA-MTX (CPM).* A solution of $(Boc\text{-}Cys\text{-}OH)_2$ (Supporting Information) (130.2 mg, 0.3 mmol), DCC (475 mg, 2.3 mmol), and DMAP (97.6 mg, 0.8 mmol) in DMSO (2 mL) was purged with nitrogen gas for 1 h and then added to DMSO (10 mL) containing PHEMA-MTX (500 mg, 0.097 mmol). The reaction was left to stir for 48 h at room temperature. The white precipitate was removed, and the crude product was added to water as a non-solvent. The dried product was obtained after lyophilization.

*Synthesis of Carboxyl-Functionalized CPM (CPM-COOH).* TEA (21.3 mg, 0.2 mmol) was poured to a well-dispersed suspension of CPM (300 mg) in DMSO (10 mL). Then, succinic anhydride (21.2 mg, 0.2 mmol) was added to the mixture, and the reaction was let to stir for 12 h at room temperature. Finally, in order to remove the unreacted succinic anhydride, the polymer was precipitated in water.

**Preparation of Janus Nanoparticles [j-(MMA-$Fe_3O_4$-CPM)].** *Preparation of CPM-COOH Microparticles and Covering Their Surfaces with Modified SPION ($NH_2$-$Fe_3O_4$-CPM).* CPM-COOH microparticles were prepared as a support for subsequent reactions. CPM-COOH microparticles were synthesized via the micro-precipitation method through adding methanol (1.5 mL) containing CPM-COOH (20 mg) dropwise into deionized water (3 mL) as a non-solvent. The mixture was stirred at a rotating speed of 250 rpm at room temperature. Amine-functionalized magnetite nanoparticles (mSPION) (see the Supporting Information) were reacted covalently with carboxylic functional groups of CPM-COOH microparticles after removing methanol by rotary evaporation. In order to activate the carboxylic groups at the surface of CPM-COOH microparticles, NHS (1.5 mg, 0.01 mmol) and EDC (2 mg, 0.01 mmol) were added to the abovementioned dispersion, and the mixture was let to continue under non-stop stirring for 1 h. Then, phosphate buffer saline (PBS) (pH = 7.4) was added to the mixture to neutralize the ambiance before replacing the whole solution to the three-necked round bottom flask equipped with a mechanical stirrer. Next, mSPIONs (30 mg) were dispersed in PBS (5 mL) and sonicated for 30 min then added dropwise to the CPM-COOH microparticle solution, and the reaction was let to continue for 24 h with a stirrer speed of 1000 rpm. Finally, unreacted CPM-COOH microparticles were removed with the help of sonication and an external magnetic field.

*Synthesis of Macro-Initiator (Br-$Fe_3O_4$-CPM).* The $NH_2$-$Fe_3O_4$-CPM microparticle (17 mg) was dispersed in dried toluene (5 mL) under sonication for 10 min, and then TEA (8.2 mg, 0.08 mmol) was added to the above dispersion under a nitrogen atmosphere. After cooling down the mixture to about 0 °C, a solution of BIBB (18.6 mg, 0.08 mmol) in toluene (1 mL) was added dropwise to the mixture during 15 min. Then, the mixture was stirred at this temperature for 6 h and continued at room temperature overnight. The mixture was washed twice with toluene and once with ethanol and finally, the macro-initiator was obtained with an external magnetic field.

*Graft Polymerization of Methyl Methacrylate from the Half Surface of Magnetite NPs.* The hybrid macro-initiator (10 mg) was dispersed in toluene (10 mL) under sonication for 10 min, and then CuBr (2.4 mg, 0.01 mmol), EBIB (3 mg, 0.015 mmol) as a sacrificial initiator, and MMA (225 mg, 2.24 mmol) were added to the above dispersion under a $N_2$ atmosphere. Next, a solution of PMDETA (2.4 mg, 0.01 mmol) in toluene (1 mL), which was purged by nitrogen gas, was poured quickly to a mixture, and the reaction was let to continue at 50 °C for 2 h. Finally, the resulting microparticles were separated by an external magnetic field and washed with toluene and ethanol, respectively.

**De-cross-linking of Microgels.** PMMA-Fe3O4-CPM Janus nanoparticles were obtained by ultrasonication of prepared microgels. To this end, a distinct amount of microgel was added to distilled water, and the mixture was exposed to US waves (50 W power, 3 s on/ 2 s off). Moreover, to approach the desirable size, waves at different times were irradiated to the mixture. Finally, the Janus NPs were collected with the help of an external magnetic field and freeze dried as well.

***In Vitro* Drug Release Studies of Janus NPss.** To investigate the drug release behavior of the US-triggered MTX-conjugated Janus NPs by a diffusion technique, 1 mg of the NP was dispersed in 2 mL of phosphate buffer saline at two different pH values of 7.4 and 5.8 and then transferred to a dialysis bag (molecular weight cut-off of 12 KD). The bag was placed into a flask containing 50 mL of fresh PBS (pH = 7.4 and 5.8) and stirred at 150 rpm and 37 °C. Next, 2 mL of the release medium was taken at district intervals and replaced with fresh PBS. The MTX release of the US-triggered Janus NP was measured by UV−vis spectroscopy at 300 nm based on the calibration curve of MTX in the same medium. The drug release percentage was determined according to the following equation (eq 1):

$$\text{drug release } (\%) = \frac{M_t}{M_0} \times 100 \tag{1}$$

$M_0$ and $M_t$ are related to the amount of the loaded and released drug at time $t$, respectively.

**Mechanism of Drug Release.** To evaluate the kinetics of the drug release process from the nanocarrier under different pH values, the release data were analyzed using the Excel add-in DDSolver program. Two types of theoretical models describing drug release from polymeric systems are Higuchi[27] and Korsmeyer−Peppas.[28] The Higuchi model describes drug release as a diffusion process based on Fick's law according to the following equation (eq 2):

$$M_t/M_\infty = K \cdot t^{0.5} \tag{2}$$

where $M_t$ and $M_\infty$ are cumulative amounts of the released drug at time $t$ and infinite time, respectively, and $K$ is Higuchi constant reflecting formulation characteristics. The Korsmeyer−Peppas model takes into account that the drug release mechanism often deviates from Fick's law and follows an anomalous behavior described by the following equation (eq 3):

$$M_t/M_\infty = K' \cdot t^n \tag{3}$$

where K′ is the kinetic constant, and $n$ is an exponent characterizing the diffusion mechanism. When pure diffusion obeys the controlling release mechanism, $n$ = 0.5, and eq 3 is converted to eq 2. Moreover, eq 2 becomes physically realistic for $n$ = 1 since the drug release follows swelling controlled release or sase II transport.[29] Both eqs 2 and 3 are short-time


https://dx.doi.org/10.1021/acsomega.0c02710
ACS Omega 2020, 5, 27119−27132

approximations of complex exact relationships and therefore, their use is confined for the description of the first 60% of the release curve. The $n$ value is used to characterize different release mechanisms as given in Table 1 for the spherical-shaped matrices.

**Table 1. Diffusion Exponent and the Solute Release Mechanism for Spherical-Shaped Matrices**

| diffusion exponent ($n$) | overall solute diffusion mechanism |
|---|---|
| $n < 0.43$ | Fickian diffusion |
| $0.43 < n < 0.8$ | anomalous (non-Fickian) diffusion |
| $0.85 < n < 1$ | case transport II |
| $n > 1$ | super case transport II |

**Characterization and Equipment.** $^1$H NMR (Bruker-Germany, 500 MHz) and Fourier-transform infrared spectroscopy (Bruker-Equinox 55 FT-IR) were used for the characterization of the polymer. The $^1$H NMR spectrum was recorded in $CDCl_3$ to confirm the structure of the initiator. Also, $^1$H NMR spectroscopy was applied to determine the structure and number average molecular weight ($M_n$) of PHEMA in DMSO. The thermal gravimetric analysis (TGA) instrument (Q50 V6.3 Build 189) was used to show the percentage of the cross-linked polymer. Samples were heated at a rate of 20 °C per min under an argon atmosphere, and the data were measured at a temperature interval of 20−600 °C. The morphology of magnetic NPs was studied by transmission electron microscopy (TEM) (Philips, CM300) at a 200 kV accelerating voltage and also scanning electron microscopy (SEM) (Hitachi S-4160 field emission SEM, operating at 20 kV). The average hydrodynamic diameter and zeta potential of NPs were estimated by dynamic light scattering (DLS) (Brookhavan, Nanobrook Omni) at 25 °C. Furthermore, UV−vis spectroscopy (Jasco-v 750) was employed to confirm the grafting of MTX to PHEMA. The optical microscopy (Leica icc50 HD) was used to verify the formation of polymeric microparticles. A SONOPULS ultrasonic homogenizer (20 kHz ± 500 Hz ultrasonic generator) model HF-GM 3200 (BANDELIN electronic GmbH & Co. KG) was used for particle dispersion, and the probe was a titanium microtip MS-72 with a diameter of 3 mm. The weight average molecular weight ($M_w$), number average molecular weight ($M_n$), and polydispersity index (PDI) of PHEMA were determined by using the gel permeation chromatography (GPC) (PL-EMD 950) with a 0.7 mL/min flow rate of *N,N*-dimethylformamide (DMF) containing 0.25% of TBAB at 25 °C. THF was used to determine the molecular weight of free PMMA, i.e., the polymer chain produced by the sacrificing initiator. The monodisperse polystyrene standards were used for calibration.

## RESULTS AND DISCUSSION

We recently set our target to prepare Janus morphology instead of a conventional core-shell structure as drug delivery carriers. This paper presents a new system based on a masking method in which, first, one of the two surface-coating polymers was cross-linked and accounted for a solid substrate to immobilize iron oxide NPs with the "grafting to" approach. In the following, the second polymer was grown based on the "grafting from" approach and modified the unreacted sides of iron oxide NPs (Scheme 1).

**Scheme 1. Total Synthetic Procedure of Janus Nanoparticles**

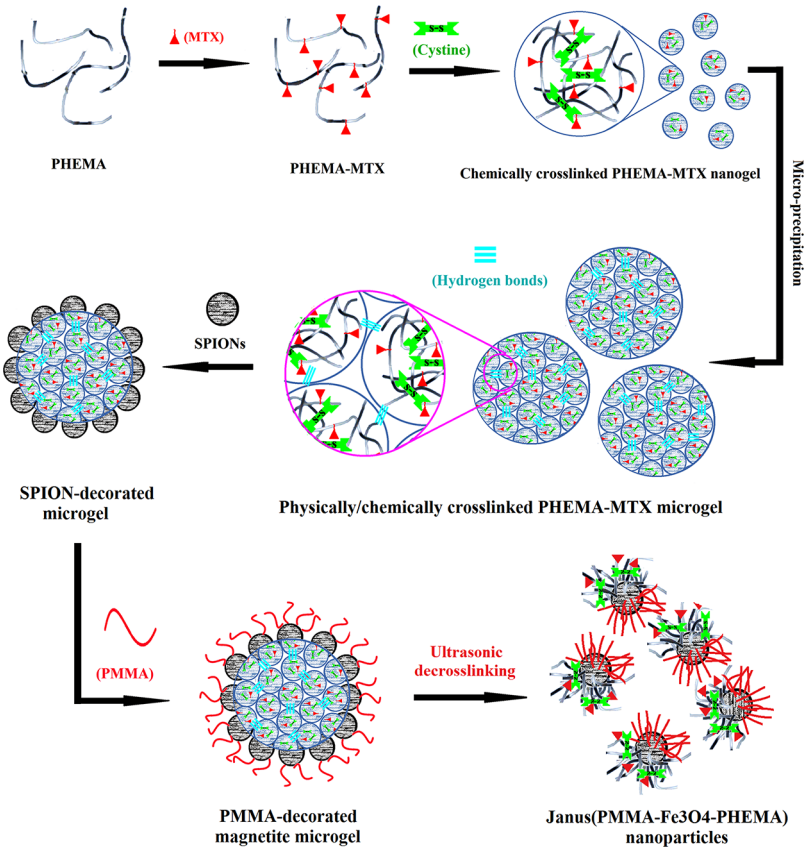




https://dx.doi.org/10.1021/acsomega.0c02710
ACS Omega 2020, 5, 27119−27132

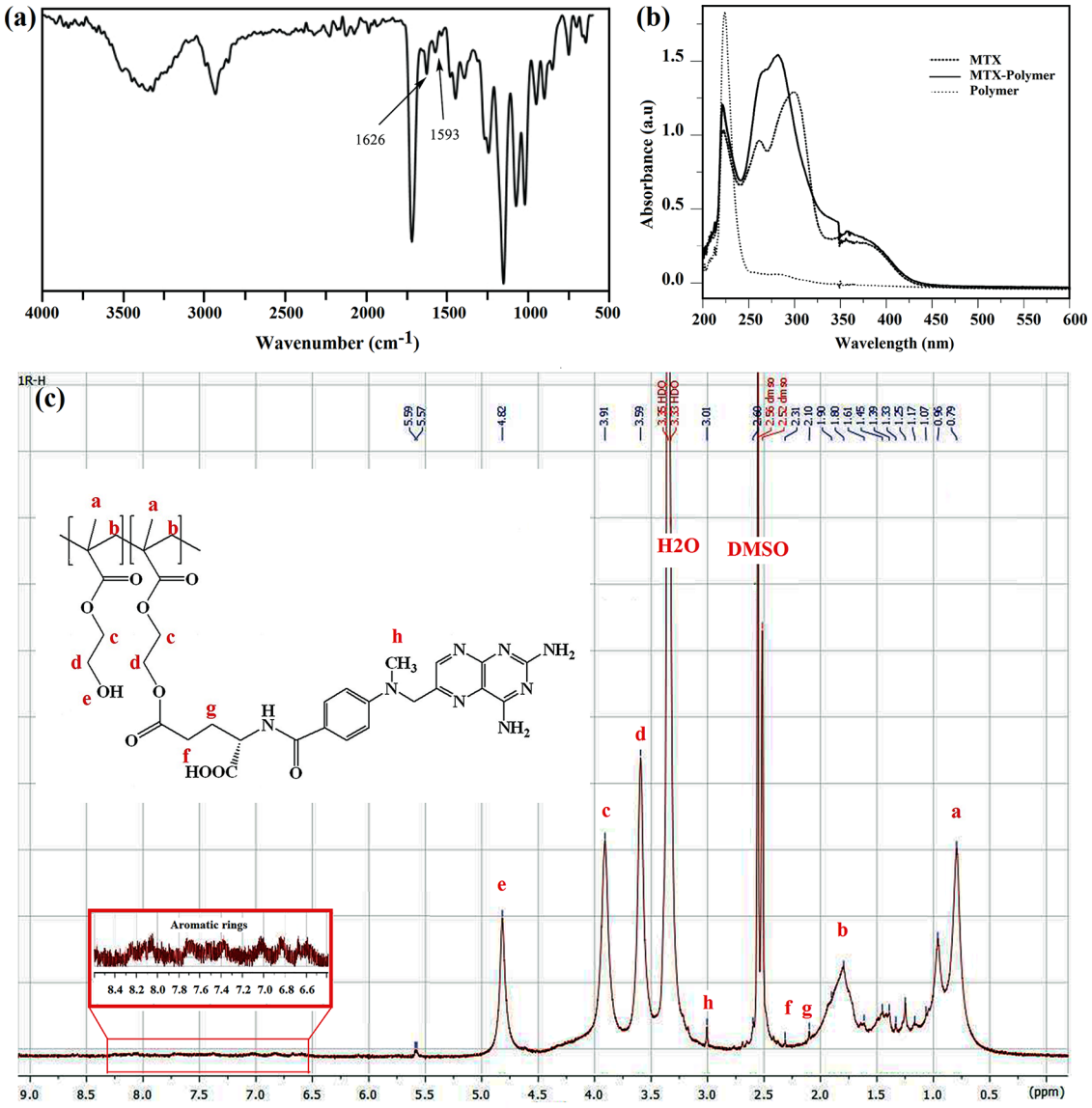


**Figure 1.** (a) FT-IR, (b) UV, and (c) $^1$H NMR spectra of PHEMA-MTX.

Here, the physically/chemically cross-linked microgels (CPM-COOH) were synthesized as the solid substrate for production of Janus NPs in subsequent reactions. The synthetic procedure used to prepare PHEMA-MTX is described in Schemes S1−S3. First, PHEMA was synthesized via ATRP of HEMA in the presence of EA-IBB as an ATRP-initiator derivative. According to Scheme S1, EA-IBB was prepared with the reaction of ethanolamine and BIBB. The FT-IR spectrum of the initiator is depicted in Figure S1. Absorption peaks at 658, 1644, 2932, and 3350 cm$^{-1}$ were attributed to the C−Br stretching, N−H bending, C−H stretching, and hydroxyl groups, respectively. In addition, the disappearance of the absorption band at 1800 cm$^{-1}$ related to acyl halide confirmed the successful preparation of the initiator. The chemical structure of EA-IBB was determined by $^1$H NMR spectroscopy in $CDCl_3$ (Figure S2). The signal at 1.96 ppm (a, 6 protons) was related to methyl protons. The peaks at 3.47 (b, 2 protons) and 3.77 (c, 2 protons) ppm were associated to the methylene protons. The signal at 7.17 ppm (d, 1 proton) was attributed to the amine proton.

PHEMA was constructed via the ATRP reaction of the 2-hydroxyethyl methacrylate monomer initiated by EA-IBB using CuBr/byp as a catalyst system (Scheme S2). The FT-IR spectrum of PHEMA is shown in Figure S3. The characteristic peak at 1717 cm$^{-1}$ was related to C═O stretching of HEMA. In addition, the peaks at 1153, 1449, and 2947 cm$^{-1}$ were attributed to the C−O stretching, C−H bending, and methylene group in PHEMA, respectively. Moreover, the peaks at 616 cm$^{-1}$, which is related to C−Br stretching, confirmed the successful synthesis of PHEMA. The $^1$H NMR spectrum of PHEMA displayed all typical proton resonance signals of HEMA repeating units (Figure S4). The peak at 0.7−0.9 ppm (a) was attributed to methyl protons in the polymer. Methylene protons of the main chain (b) were revealed at 1.8 ppm. The signals at 3.5, 3.8, and 4.8 ppm were assigned to methylene protons (c and d) and $CH_2OH$ in HEMA.[30] In addition, methylene protons of the initiator (e) were located at 3 ppm. The number average molecular weight of PHEMA was about 3000 g/mol obtained by $^1$H NMR spectroscopy. The GPC was used to determine the $M_n$, $M_w$, and PDI of PHEMA. The polymer was dissolved in DMF, and


https://dx.doi.org/10.1021/acsomega.0c02710
ACS Omega 2020, 5, 27119−27132

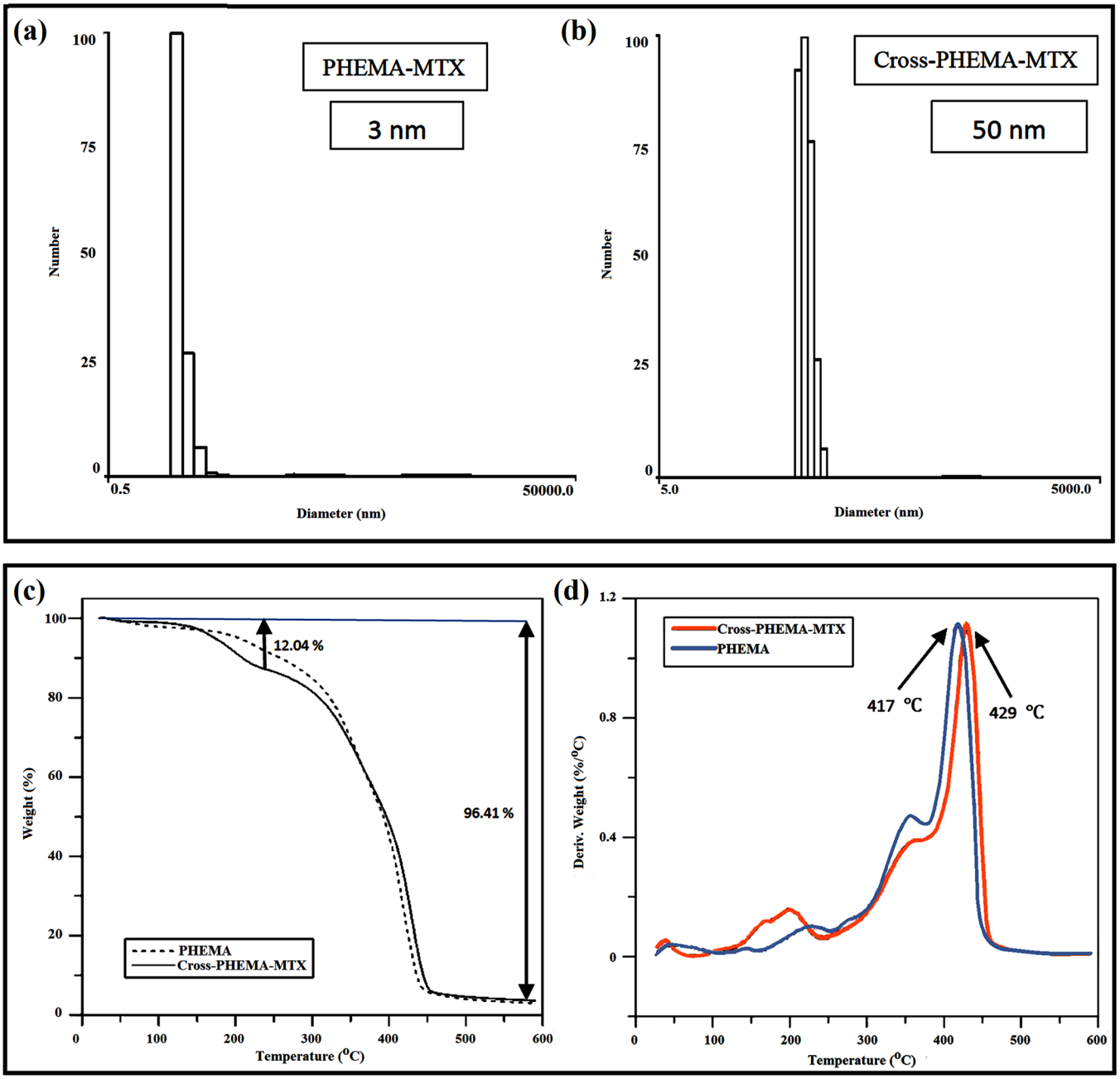


**Figure 2.** Particle size of (a) PM and (b) CPM. (c) TGA and (d) DTG thermograms of PHEMA and CPM.

the GPC was carried out in a flow rate of 0.7 mL/min at 25 °C. The GPC results showed that the $M_n$, $M_w$, and PDI were 3.55 KDa, 4.72 KDa, and 1.33, respectively (Figure S5). MTX, which has a similarity to folic acid, is able to inhibit dihydrofolate reductase (DHFR), leading to decreased cell viability and cell death. MTX has proven to be an effective targeting agent due to the presence of folate receptors on the cell membranes of different kinds of cancer cells.[31] Therefore, in order to increase the smartness of nanoparticles, MTX was chemically grafted to the PHEMA through esterification reaction (Scheme S3).

The FT-IR spectrum of PHEMA-MTX depicts two new peaks at 1593 and 1626 $cm^{-1}$, which were attributed to the stretching vibration of the aromatic ring and free carboxylate groups in MTX, respectively (Figure 1a). Moreover, UV−vis spectroscopy was utilized to confirm the successful synthesis of PHEMA-MTX. According to Figure 1b, the main absorption bounds of PHEMA-MTX shifted to 267 and 284 nm compared to those of pure MTX, which were revealed at 264 and 303 nm, respectively. The structure of PHEMA-MTX was determined by $^1$H NMR spectroscopy in DMSO (Figure 1c), and new peaks appeared at $\delta$ = 2.1−2.31 and 3.01 ppm, which belonged to methylene and methyl protons of MTX-conjugated PHEMA. Also, the peaks at $\delta$ = 6.5−8 ppm were related to aromatic rings of MTX. The MTX/polymer weight ratio was calculated by integrating the methylene protons (c and d) in the PHEMA and found to be 33.76 (wt %) (Figure S6).

In order to form cross-linked PHEMA-MTX (CPM), which was used as a micro-substrate for preparation of Janus NPs in subsequent reactions, $(Boc\text{-}Cys\text{-}OH)_2$ was first synthesized as the cross-linker (Scheme S4) according to our previously


https://dx.doi.org/10.1021/acsomega.0c02710
ACS Omega 2020, 5, 27119−27132

reported method.[32] $(Boc\text{-}Cys\text{-}OH)_2$ was prepared through the reaction of di-*tert*-butyl dicarbonate with cystine, and the product was characterized by FT-IR and $^1H$ NMR spectroscopy (data not shown). According to the FT-IR spectrum of the cross-linker, the strong absorption peak at 1725 $cm^{-1}$ and the broad peak at 2800−3400 $cm^{-1}$ were assigned to carbonyl stretching and O−H absorption of carboxylic acid group attending the cross-linker, respectively. Moreover, the peaks at 1251, 1515, and 1368 $cm^{-1}$ were attributed to the C−O stretching, N−H bending, and methylene group in the cross-linker, respectively. The $^1H$ NMR spectrum of $(Boc\text{-}Cys\text{-}OH)_2$ shows a singlet peak at 1.6 ppm, which was ascribed to methyl protons of *tert*-butyl groups. In addition, the methylene and methane peaks of the cross-linker were revealed at 2.9−3.1 and 3.6 ppm, respectively. PHEMA-MTX (PM) was slightly cross-linked with the help of $(Boc\text{-}Cys\text{-}OH)_2$ as the cross-linker and in the presence of DCC and DMAP for 48 h (Scheme 1). In drug delivery systems, the size of final nanogels is so important because it should be less than 100 nm to be used as a nanocarrier. Therefore, at the beginning, it was supposed to prepare cross-linked PHEMA-MTX with an average size of 50 nm, which has a more reasonable distance than the boundary of 100 nm. To this end, samples of CPM were prepared with different polymer/cross-linker ratios, and it was clear that the nanogel size was positively correlated with the amount of cross-linking (decrease in cross-linking led to decrease in the size of nanogel). This controlled cross-linking helped enhance the molecular weight of PHEMA while the hydrophilicity of CPM was somewhat maintained. The CPM was characterized by means of DLS and TGA. The particle size of CPM and PM dispersion in methanol was measured by DLS. As shown in Figure 2a, the average hydrodynamic diameter of PHEMA-MTX after cross-linking reached to about 50 nm, which confirmed the successful preparation of cross-linked PHEMA-MTX nanoparticles. The TGA analysis indicates that CPM nanoparticles were synthesized correctly (Figure 2b). According to the TGA curve of CPM nanoparticles, a distinct weight loss appeared before 250 °C, which is attributed to MTX degradation. As the TGA curves of PHEMA and CPM overlapped after 250 °C, derivative thermogravimetry (DTG) of PHEMA and CPM was investigated to confirm the correct synthesis of cross-linked PHEMA-MTX nanoparticles. As depicted in DTG curves, the maximum temperature of PHEMA degradation stood at about 417 °C, while this temperature shifted to 429 °C for CPM nanoparticles, indicating the slight cross-linking of PHEMA-MTX.

The surface of CPM nanoparticles was subsequently modified by succinic anhydride in the presence of TEA (Scheme S5). To confirm the successful preparation of CPM-COOH, an identical amount of PHEMA, CPM, and CPM-COOH was separately dispersed in methanol, and their zeta potential data were evaluated. The average zeta potential of CPM-COOH nanoparticles dwindled noticeably from −4 for PHEMA to −8 and −20 for CPM and CPM-COOH, respectively, indicating the existence of carboxylic groups at the surface of CPM nanoparticles.

Consequently, micron-sized CPM-COOH gels were formed via physically/chemically cross-linking of nanoparticles. In order to prepare the polymeric substrates of CPM-COOH, the methanolic solution of CPM-COOH was poured dropwise to water, and the coagulated CPM-COOH in water was achieved after evaporation of methanol. The optical microscopy was utilized to confirm the process of preparation and the coagulation of CPM-COOH microparticles. According to the obtained result from optical microscopy, particles were prepared with dimension more than 20 $\mu$m (Figure 3a).

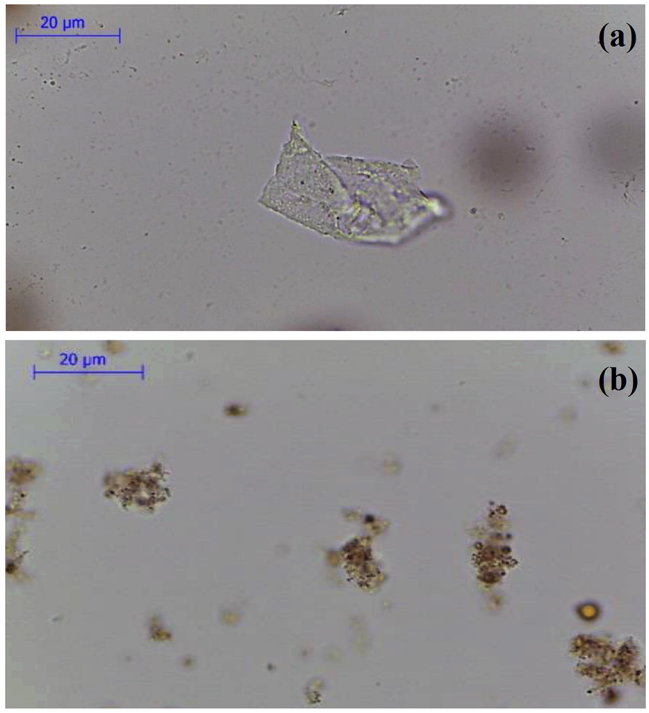


**Figure 3.** Optical microscopy images of (a) coagulated CPM-COOH and (b) mSPION-coated CPM-COOH microparticles.

Figure 4a depicts the TEM image of the chemically cross-linked PHEMA nanogel. Similar to DLS results (Figure 2a), which indicated the average hydrodynamic diameter of CPM, it is clear that the average size of PHEMA-MTX increased to around 40 nm after cross-linking. Although a little coagulation is displayed in the TEM image of the CPM nanogel, the spherical shape of nanoparticles is yet observable (Figure 4a). This coagulation enhanced noticeably due to the physical attachment of nanogels, leading to the construction of the CPM microparticles without a specified shape and form with a spiky surface (Figure 4b, red arrows).

**Preparation of Magnetite Nanoparticles.** The magnetite nanoparticles were prepared by a co-precipitation method. Synthesized SPIONs were modified with APTES to prepare amine-functionalized SPIONs (Scheme S6). APTES-modified magnetic NPs acted as a core for heterogeneously attaching two polymers with "grafting from" and "grafting to" approaches. The FT-IR spectrum of bare super paramagnetic iron oxide nanoparticles (SPIONs) is shown in Figure S7. The peak at 588 $cm^{-1}$ is related to the bending vibration of Fe−O as the characteristic peak. The stretching vibration of the O−H bond attached on the surface of SPIONs was revealed at 3200 $cm^{-1}$. Figure S8 shows the FT-IR spectrum of APTES-modified magnetic nanoparticles (mSPION). The presence of peaks at 3337 and 1563 $cm^{-1}$ was attributed to the N−H stretching and bending vibration, respectively. The Si−O stretching vibration was seen at 1049 $cm^{-1}$. The peaks at 2890, 1107, and 1490 $cm^{-1}$ were assigned to the C−H stretching, C−N stretching, and C−H bending vibration, respectively.

The morphology and size of bare SPIONs and APTES-modified SPOINs were investigated using SEM and DLS


https://dx.doi.org/10.1021/acsomega.0c02710
ACS Omega 2020, 5, 27119−27132

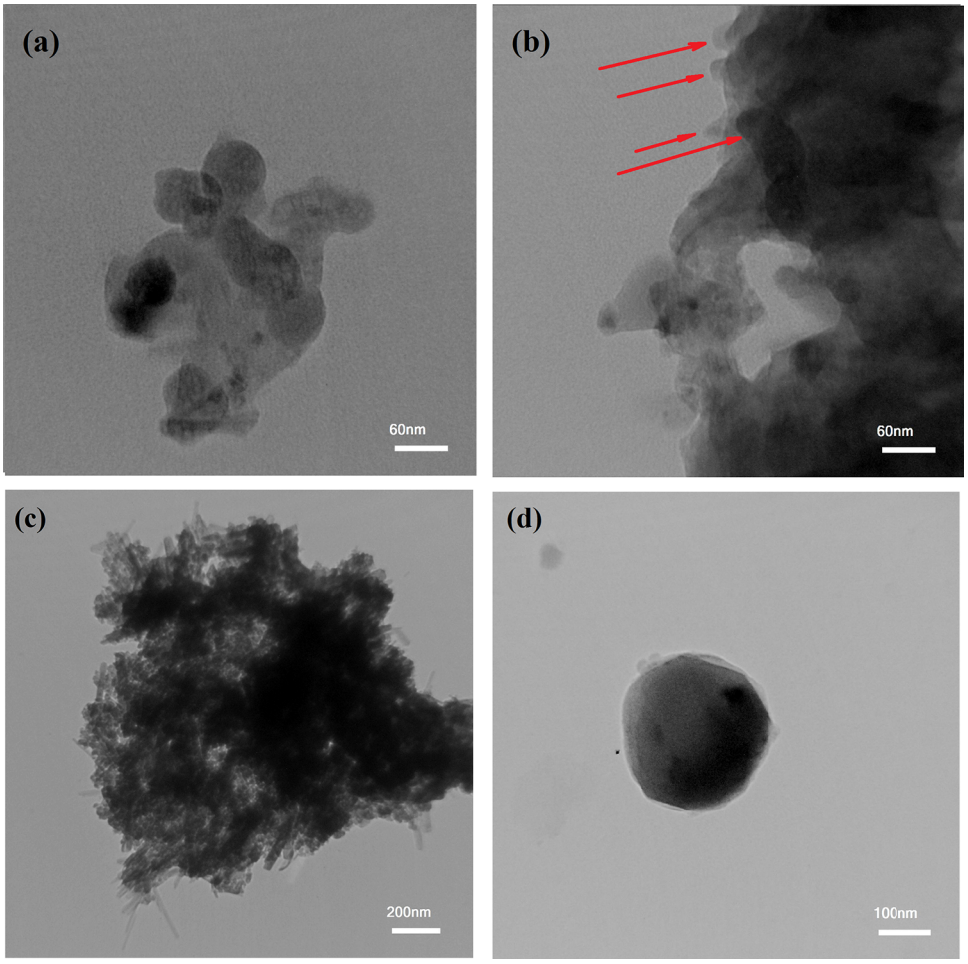


**Figure 4.** TEM images of (a) chemically cross-linked PHEMA nanogel, (b) physically/chemically cross-linked PHEMA microgel, (c) mSPION-coated CPM-COOH microparticles, and (d) Janus (PMMA-$Fe_3O_4$-PHEMA) obtained after 20 min of US irradiation.

analyses. As shown in SEM images (Figure S9), the bare SPOINs with a size of 20−30 nm had a spherical structure and uneven surface. While the ATPES-modified SPOINs (mSPION) maintained their spherical structure, the amount of agglomeration decreased in these NPs. The numerical values of size corresponding to the magnetite nanoparticles and their amine-modified derivative are presented in Figure S10. The SEM sizes of nanoparticles are smaller than those obtained via DLS analyses because DLS measures the hydrodynamic diameter, while SEM determines the size of dried particles. However, some aggregation was expected to occur during the size measuring of the nanoparticle dispersions by the DLS technique at neutral pH (Figure S10).

**Covering the Surface of CPM-COOH Microparticles with Magnetite Nanoparticles (NH2-Fe3O4-CPM).** The Janus nanoparticles were synthesized through the masking method. In the first step of preparation, the mSPIONs were chemically attached on the surface of CPM-COOH microparticles ("grafting to" approach). To this end, the well-dispersed mixture of modified iron oxide nanoparticles was added to polymeric solution of CPM-COOH microparticles in the presence of EDC/NHS. According to Scheme 1, some parts of mSPION functional groups reacted with carboxylic groups attending the surface of CPM-COOH microparticles. The intact functional groups remained on the surface of mSPION were available for subsequent reactions. Optical microscopy was utilized to investigate the morphology and uniformity of the as-prepared modified magnetite-coated microparticles of CPM-COOH (Figure 3b). It is believed that mineral compositions have a significant impact on the swelling reduction of hydrogels.[33] As a result, the dimensions of microparticles decreased by attaching mSPION on the surface of CPM-COOH microparticles. Figure 4c depicts TEM images of mSPION-coated CPM-COOH microparticles. According to this picture, the half surface of modified SPIONs was masked by chemical surface deposition of amine-decorated magnetite NPs on the CPM-COOH microparticles and made it possible to use the residue active sites to complete subsequent reactions and prepare Janus NPs. Moreover, Figure S11 shows a high-magnification TEM image and SAED pattern of mSPION-coated CPM-COOH microparticles. According to this picture, there are nanoparticles with the average size of 8−12 nm on the surface of mSPION-coated CPM-COOH microparticles (Figure S11a), as well as the indexed rings, confirm the presence of magnetite nanoparticles (Figure S11b).

In the second step of preparation of Janus nanoparticles, MMA monomers grew on the remained active sites of modified iron oxide NP-coated CPM-COOH microparticles. To this end, it was necessary to prepare a macro-initiator (Br-$Fe_3O_4$-CPM) through the reaction of mSPION-coated CMP-COOH microparticles ($NH_2$-$Fe_3O_4$-CPM) and BIBB in the presence of TEA for 24 h (Figure 5a). Energy dispersive X-ray spectroscopy (EDX) was used to analyze the elementary


https://dx.doi.org/10.1021/acsomega.0c02710
ACS Omega 2020, 5, 27119−27132

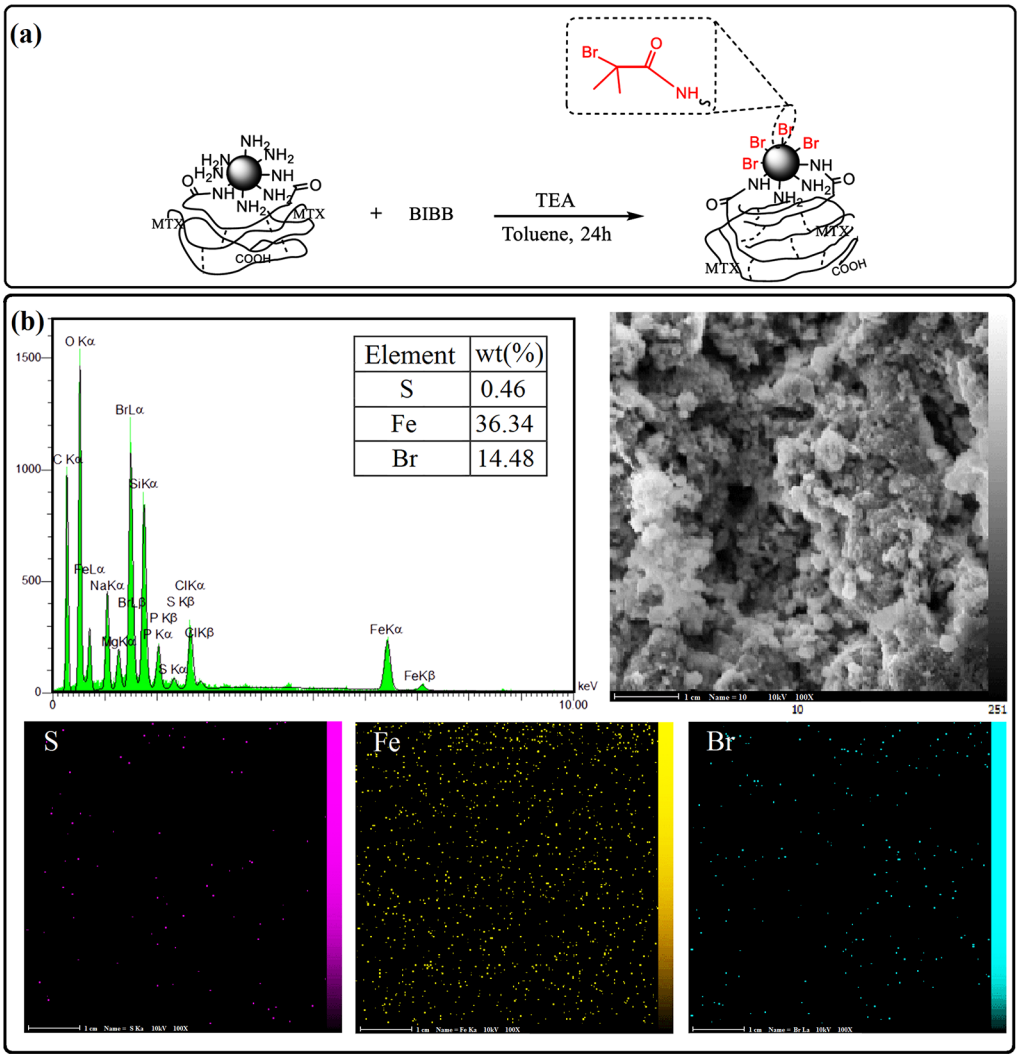


**Figure 5.** (a) Synthetic procedure of macro-initiator. (b) EDX pattern and SEM elemental mapping of the Br-$Fe_3O_4$-CPM.

composition of the Br-$Fe_3O_4$-CPM sample. The EDX pattern (Figure 5b) showed the signal of S, Fe, and Br with atomic percentages of 0.46, 36.34, and 14.48%, respectively. Moreover, the SEM−EDX mapping was conducted to study the elemental distribution for the Br-$Fe_3O_4$-CPM macro-initiator, and it can be observed that S, Fe, and Br elements are evenly dispersed on the surface of the entire microparticle.

The TGA and DTG curves of $NH_2$-Fe-CPM are given in Figure 6a. The sample was freeze dried for 72 h and then used for TGA analysis very quickly. According to the DTG thermogram, it is clear that there are three distinct peaks. From the TGA thermogram, it was amazing that a peak appeared under 150 °C despite freeze drying for 72 h. Without any doubt, this was not related to water release. Looking more closely at other reports, it can be seen that cysteine derivatives release $CO_2$ at 100−130°C.[34] Therefore, it just could be assigned to the weight loss of the cross-linker (3.95%). The second mass loss (4.75%) was observed between 170 and 350 °C, and the last one appeared after 350 °C. These two peaks are related to the degradation of MTX and PHEMA, respectively. Moreover, the amount of the MTX/polymer ratio was 35.31% calculated based on Figure 6a, which was close to the NMR result.

Finally, PMMA-decorated magnetite nanogels were prepared trough "grafting from" polymerization of MMA monomers on the surface of the macro-initiator in the presence of EBIB as the sacrificial initiator (Scheme 1). By exposing the dual-polymer-modified microgels to the US waves, the physical bonds of microparticles were broken and converted to the Janus nanoparticles correctly. To reduce the size of the final particle to a desirable dimension that has an application in drug delivery, the microgel was exposed to the US irradiation at different times. To begin, the microgel was dispersed in deionized water under ultrasonic irradiation for 15 min. Therefore, double peaks appeared in the DLS result, one is in the nanometer dimension and the other in micrometric size (Figure 7a). When the intensity of US waves was enhanced to 20 min, only a single peak has appeared in the DLS curve with an average hydrodynamic diameter of 366 nm and a standard deviation (SD) of 62 nm (Figure 7b). It is interesting to note that when the microgel was exposed to US waves for 25 min, it was converted to a nanoparticle with an average hydrodynamic diameter of 109 nm, and the SD reached 4.7 nm (Figure 7c). However, significant size reduction was not observed by exposing the microparticles to the US waves for 30 min. The US-triggered nanoparticles were exposed immediately to the external magnetic field; so,


https://dx.doi.org/10.1021/acsomega.0c02710
ACS Omega 2020, 5, 27119−27132

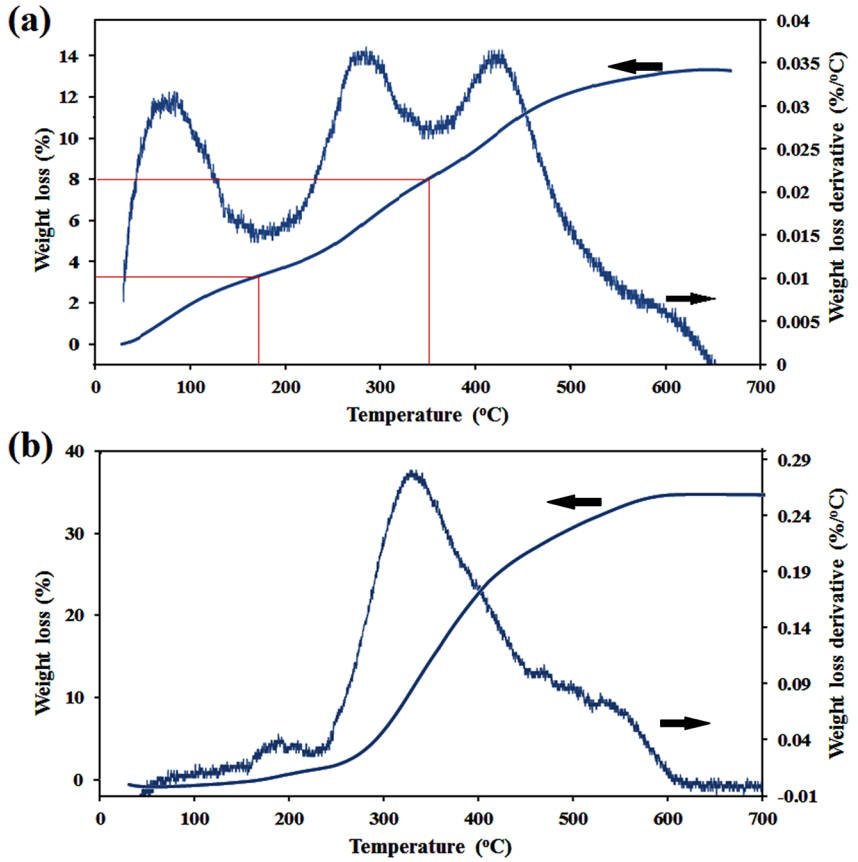


**Figure 6.** TGA and DTG thermograms of (a) $NH_2$-Fe-CPM and (b) (PMMA-$Fe_3O_4$-PHMA) Janus NPs samples.

just the outer layers of hybrid nanoparticles containing both polymers and magnetite nanoparticles were separated by the external magnetite field. As a result, some inner parts of microparticles, which did not have any SPIONs and indubitably enough opportunity to react with PMMA, could not have been separated by the external magnetite field. This can be seen in the thermal behavior of PMMA-$Fe_3O_4$-PHEMA NPs after freeze drying for 72 h (Figure 6b). About 65.12% of the total weight stayed unspoiled, which is related to magnetite attending in NPs. It might seem that the amount of SPION in Figure 6b differs from that of Figure 6a. However, it is not true, and the weight of the SPION had no change. In fact, that change was related to the amount of the polymer. According to the amount of SPION in two TGA results, the weights of PHEMA-MTX and PMMA were 10.12 and 24.76%, respectively. In this way, the amount of drug loading in final NPs was 3.57%.

According to the FT-IR spectrum of the (PMMA-$Fe_3O_4$-PHEMA) Janus nanoparticle (Figure 7d), it can be seen that the two bands have appeared at 1381 and 743 $cm^{-1}$ related to the $\alpha$-methyl group vibrations of both polymers. The peak at 898 $cm^{-1}$ is the characteristic absorption vibration of PMMA along with the band at 980 $cm^{-1}$. Finally, the peak at 2980 $cm^{-1}$ can be attributed to the C−H bond stretching vibration of the $-CH_3$ group.[35] These new peaks confirm the correct polymerization of MMA monomers on the surface of the macro-initiator.

Magnetic properties of PMMA-$Fe_3O_4$-PHEMA was measured by VSM at room temperature and compared to bare magnetite nanoparticles (Figure 8a). As observed from VSM results, the bare SPION and final NPs exhibited a magnetization of 55 and 15, respectively, and no hysteresis loop was indicated in the magnetization curve ($H_c$ = 0 Oe). Moreover, the upward trend in the amount of saturation magnetization of PMMA-$Fe_3O_4$-PHEMA in comparison with bare SPIONs was assigned to the attachment of polymers (PMMA and PHEMA) to the surface of SPIONs. These values demonstrate that both samples have a superparamagnetic nature. To demonstrate the magnetic separability of Janus nanoparticles, a dispersion of PMMA-$Fe_3O_4$-PHEMA nanoparticles in water was exposed to an ultrasonic probe, and then a magnet was placed near one side of the glass bottle; the polymer-coated nanoparticles were collected in less than 1 min (Figure 8b).

TEM images of US-triggered Janus NPs show a different contrast compared to that of the previous stage, which means that ATRP of MMA monomers took place successfully on the active sites of iron oxide nanoparticles (Figure 4d).

Finally, PDI and $M_n$ of PMMA were measured based on the sacrificial initiator and found to be 1.27 and 11,600, respectively. It was verified that the molecular weight and polydispersity of the free polymer produced from the sacrificial initiator is in good agreement with the characteristics of the graft polymer.[36]

The *in vitro* release of MTX from the PMMA-$Fe_3O_4$-PHEMA Janus NP was conducted in PBS at pH values of 7.4 and 5.8 at the same temperatures of 37 °C to mimic the physiological condition. pH-sensitive nanoparticles were designed to release the loaded drug at the pH value of cancerous cells (pH <7.4). Drug release profiles of the PMMA-$Fe_3O_4$-PHEMA Janus NP were calculated at pH values of 7.4 (physiological condition) and 5.8 to assess the sensitivity of this nanoparticle. The MTX release rate at pH 5.8 was higher


https://dx.doi.org/10.1021/acsomega.0c02710
ACS Omega 2020, 5, 27119−27132

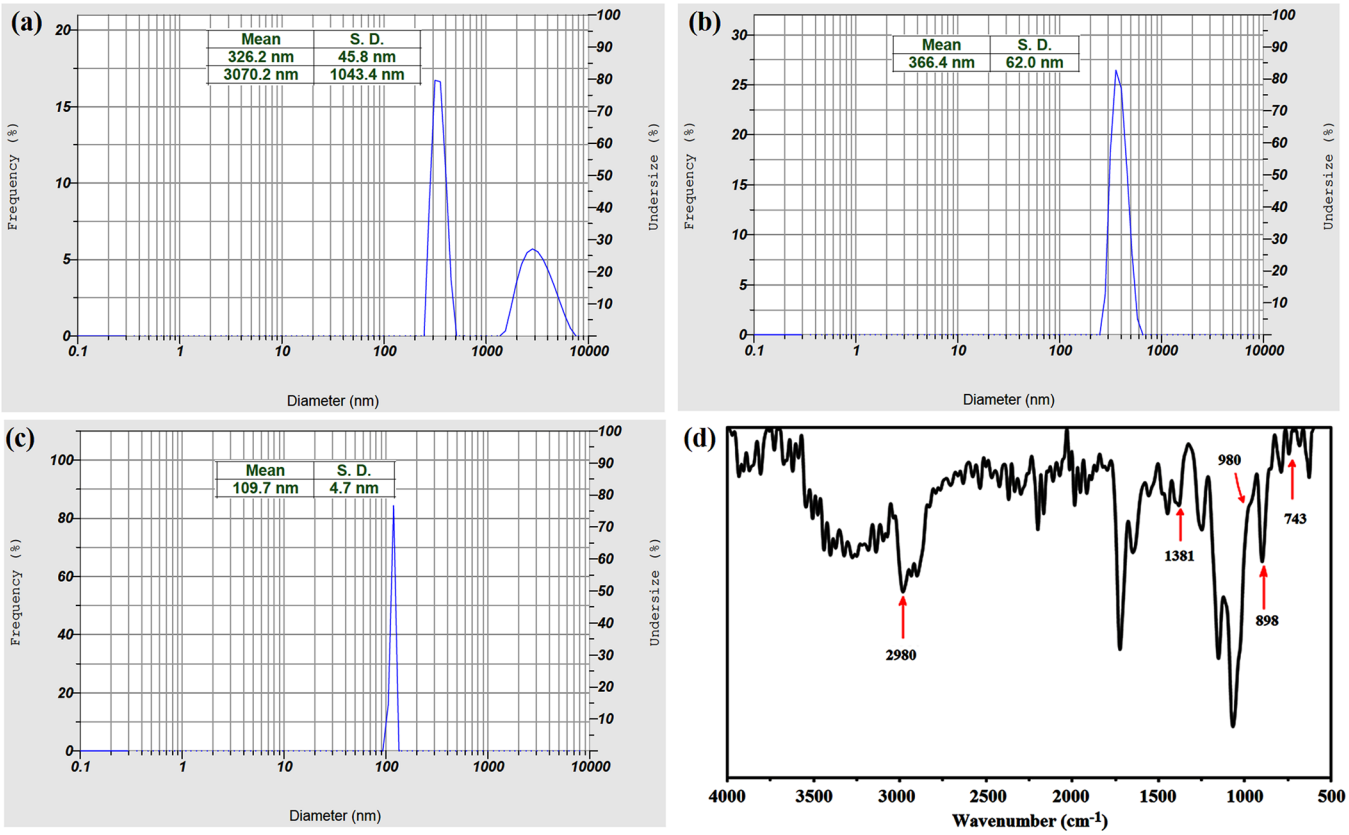


**Figure 7.** Average hydrodynamic diameter of NPs after exposing to US waves for (a) 15, (b) 20, and (c) 25 min. (d) FT-IR spectrum of the (PMMA-$Fe_3O_4$-PHEMA) Janus nanoparticle.

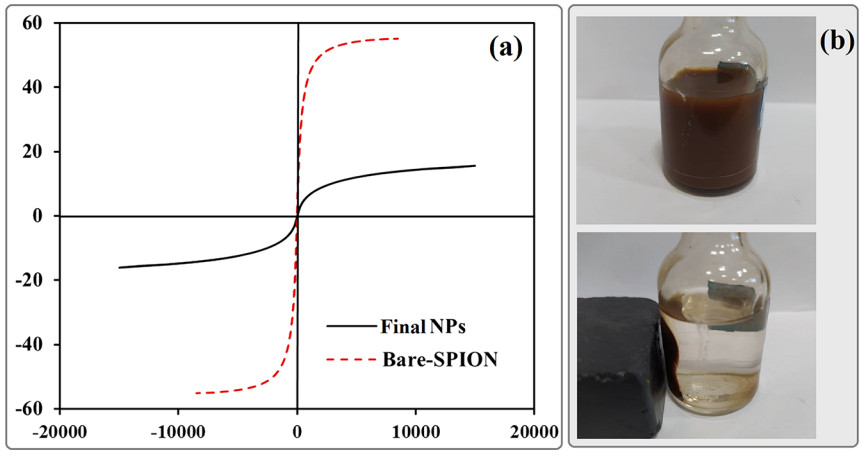


**Figure 8.** (a) Magnetic hysteresis loops of bare and final Janus NPs. (b) Separation of Janus NPs from their suspension in water by an external magnetic field.

than that at pH 7.4, which was due to the hydrolysis of MTX under an acidic condition.[37] According to Figure 9, by the release profiles of the nanoparticle, about 60% of MTX was released from the nanoparticle under the acidic condition in 170 h compared to 25% in physiological media. Moreover, the gentle release of MTX at the first hours of the study is related to the drug molecules, which were trapped between polymer chains of the nanoparticles through hydrogen bonding.

**Evaluation of Drug Release Kinetics.** To get insight into the release mechanism of MTX from PMMA-Fe3O4-PHEMA Janus NPs, the release data were fitted into Korsmeyer−Peppas and Higuchi equations. The Higuchi's release rate constants ($K$), the Korsmeyer−Peppas release rate constants ($K'$), and release exponents ($n$) were calculated from eqs 2 and 3, respectively, and their results are summarized in Table 2. Moreover, as is shown in Korsmeyer−Peppas fits (Figure S12), to determine the accuracy of the fit, correlation coefficient ($r^2$) values were calculated using the Excel add-in DDSolver program. The kinetic release study results confirmed that the MTX release of the Janus NP in pH 7.4 showed Fickian diffusion at both stages. The kinetic release study at pH 5.8 showed noticeable results. MTX release of the Janus NP at the first stage obeyed Fickian diffusion, while the drug release mechanism at the second stage deviated from Fick's law and


https://dx.doi.org/10.1021/acsomega.0c02710
ACS Omega 2020, 5, 27119−27132

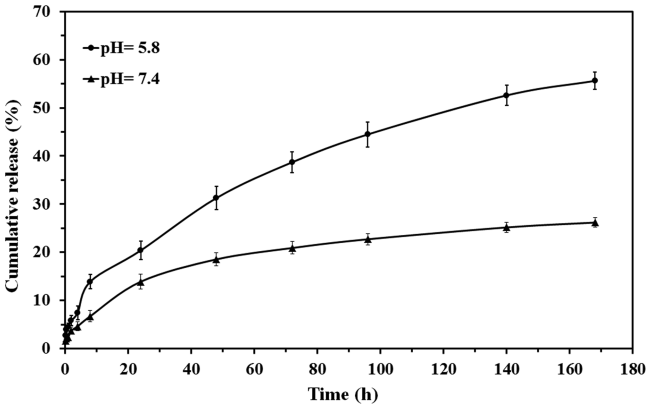


**Figure 9.** *In vitro* release of MTX from the PMMA-$Fe_3O_4$-PHEMA Janus NP.

followed an anomalous behavior. Based on the structure of the nanoparticle, it is believed that the release rate of the drug at pH 5.8 (second stage) is controlled by both the rate of hydrolysis of the ester bond between the PHEMA-drug and its rate of diffusion.[38]

## CONCLUSIONS

In the present study, we utilized hydrophilic PHEMA, hydrophobic PMMA, and SPIONs to prepare a stimuli-responsive magnetic nanocarrier with Janus morphology. To this end, low-molecular-weight PHEMA was synthesized through the ATRP method. Then, MTX as an anti-cancer drug was grafted to the polymer, which generally increases the sensitivity of final NPs. In order to prepare the micro-substrate, MTX-grafted PHEMA was cross-linked slightly. As the size of final Janus NPs was so important, CPM with an average size of 50 nm was prepared through optimizing the ratio of the drug-conjugated polymer to the cross-linker. In this way, the prepared nanogels showed a little hydrophilic property. In the next step, micron-sized CPM-COOH gels were formed via the seed growth method. Optical microscopy was utilized to confirm the process of preparation and the coagulation of CPM-COOH microparticles. Then, modified SPIONs were immobilized on the surface of the micro-substrate. The micro-initiator was prepared through modification of unreacted sites of immobilized SPIONs. The EDS analysis confirmed the successful preparation of the micro-initiator. Finally, PMMA gradually grew on the surface of the micro-initiator in the presence of a sacrificial initiator. The size of the final Janus nanogel reached 109 nm after chemically linking the PMMA layer on the top surfaces of previously deposited magnetite NPs. Optimum US waves were irradiated to the microgel to prepare (PMMA-$Fe_3O_4$-PHEMA) Janus NPs with desirable size. According to TEM images, Janus NPs have two distinct areas, which means that our final structure was synthesized correctly. The MTX release of US-triggered Janus NPs showed that the nanoparticle was responsive to acidic conditions. The release data were analyzed using the Excel add-in DDSolver program to evaluate the kinetics of the drug release process from the nanocarrier under different pH values, and the result showed that the release rate of the drug at pH 5.8 (second stage) is controlled by both the rate of hydrolysis of the ester bond between PHEMA-drug and its rate of diffusion.

## ASSOCIATED CONTENT

### Supporting Information

The Supporting Information is available free of charge at https://pubs.acs.org/doi/10.1021/acsomega.0c02710.

Synthesis of 2-bromo-*N*-(2-hydroxyethyl)-2-methylpropanamide (EA-IBB) (ATRP initiator); synthesis of (Boc-Cys-OH)2 as the cross-linker; synthesis of magnetite nanoparticles (SPIONs); synthesis of amino-functionalized magnetic nanoparticles with APTES (mSPION); FT-IR spectrum of the EA-IBB initiator; $^1$H NMR spectrum of the EA-IBB initiator; FT-IR spectra of PHEMA; $^1$H NMR spectrum of PHEMA; GPC chromatogram for PHEMA made by ATRP; MTX/polymer ratio calculated by integrating the methylene protons (c and d) in PHEMA; FT-IR spectra of the SPION; FT-IR spectra of the mSPION; SEM images of (a) SPION and (b) mSPION; particle size of (a) SPION and (b) mSPION obtained from DLS analysis at pH = 7; (a) TEM image of mSPION-coated CPM-COOH microparticles with higher magnification and (b) SAED pattern of mSPION-coated CPM-COOH microparticles; Korsmeyer−Peppas diagrams of MTX release from the PMMA-Fe3O4-PHEMA Janus NP at (a) stage 1, pH 5.8, (b) stage 2, pH 5.8, (c) stage 1, pH 7.4, and (d) stage 2, pH 7.4; synthesis of EA-IBB; synthesis of PHEMA; synthesis of PHEMA-MTX; synthesis of $(Boc\text{-}Cys\text{-}OH)_2$ as the cross-linker; synthetic procedure of CPM-COOH; and synthesis of SPION (step 1) and mSPION (step 2) (PDF)

## AUTHOR INFORMATION

### Corresponding Author

**Sepideh Khoee** − *Polymer Laboratory, School of Chemistry, College of Science, University of Tehran, Tehran 1417466191, Iran;* orcid.org/0000-0001-7297-8743; Phone: (098) 21 61113301; Email: khoee@khayam.ut.ac.ir; Fax: (098) 2166495291

**Table 2. Summary of Fitting Model Parameters of MTX Release Data from the PMMA-Fe3O4-PHEMA Janus NP**

| | | model | | | | | |
|---|---|---|---|---|---|---|---|
| | | Higuchi | | Korsmeyer−Peppas | | | |
| pH | stage | $K$ | $r^2$ | $K'$ | $r^2$ | $n$ | drug transport mechanism |
| 5.8 | 1 | 4.825 | 0.9775 | 4.95 | 0.9964 | 0.32 | Fickian diffusion |
| | 2 | 4.673 | 0.9976 | 4.858 | 0.9977 | 0.49 | anomalous diffusion |
| 7.4 | 1 | 2.839 | 0.9835 | 2.883 | 0.9873 | 0.4 | Fickian diffusion |
| | 2 | 2.415 | 0.9719 | 3.875 | 0.9827 | 0.39 | Fickian diffusion |



https://dx.doi.org/10.1021/acsomega.0c02710
ACS Omega 2020, 5, 27119−27132

### Authors

**Rahim Ghanbarinia Firozjah** − *Polymer Laboratory, School of Chemistry, College of Science, University of Tehran, Tehran 1417466191, Iran*

**Amirhossein Sadeghi** − *Polymer Laboratory, School of Chemistry, College of Science, University of Tehran, Tehran 1417466191, Iran*

Complete contact information is available at: https://pubs.acs.org/10.1021/acsomega.0c02710


### Notes

The authors declare no competing financial interest.

## ■ ACKNOWLEDGMENTS

The authors are most grateful for the financial support of this research project by the University of Tehran.

## ■ REFERENCES


(1) Khoee, S.; Sadeghi, A. An NIR-Triggered Drug Release and Highly Efficient Photodynamic Therapy from PCL/PNIPAm/Porphyrin Modified Graphene Oxide Nanoparticles with the Janus Morphology. *RSC Adv.* **2019**, *9*, 39780−39792.

(2) Melgar-Lesmes, P.; Luquero, A.; Parra-Robert, M.; Mora, A.; Ribera, J.; Edelman, E. R.; Jiménez, W. Graphene-Dendrimer Nanostars for Targeted Macrophage Overexpression of Metalloproteinase 9 and Hepatic Fibrosis Precision Therapy. *Nano Lett.* **2018**, *18*, 5839−5845.

(3) Houssami, N.; Turner, R. M.; Morrow, M. Meta-Analysis of Pre-Operative Magnetic Resonance Imaging (MRI) and Surgical Treatment for Breast Cancer. *Breast Cancer Res. Treat.* **2017**, *165*, 273−283.

(4) Polyak, B.; Friedman, G. Magnetic Targeting for Site-Specific Drug Delivery: Applications and Clinical Potential. *Expert Opin. Drug Deliv.* **2009**, *6*, 53−70.

(5) Bhowmick, A.; Saha, A.; Pramanik, N.; Banerjee, S.; Das, M.; Kundu, P. P. Novel Magnetic Antimicrobial Nanocomposites for Bone Tissue Engineering Applications. *RSC Adv.* **2015**, *5*, 25437−25445.

(6) Mosayebi, J.; Kiyasatfar, M.; Laurent, S. *Synthesis, Functionalization, and Design of Magnetic Nanoparticles for Theranostic Applications. Adv. Healthcare Mater.* 2017; *6*(23), 1700306, DOI: 10.1002/adhm.201700306.

(7) Weaver, J. V. M.; Bannister, I.; Robinson, K. L.; Bories-Azeau, X.; Armes, S. P.; Smallridge, M.; Mckenna, P. Stimulus-Responsive Water-Soluble Polymers Based on 2-Hydroxyethyl Methacrylate. *Macromolecules* **2004**, 2395−2403.

(8) Zobel, H. P.; Stieneker, F.; Atmaca-Abdel Aziz, S.; Gilbert, M.; Werner, D.; R. Noe, C.; Kreuter, J.; Zimmer, A. Evaluation of Aminoalkylmethacrylate Nanoparticles as Colloidal Drug Carrier Systems. Part II: Characterization of Antisense Oligonucleotides Loaded Copolymer Nanoparticles. *Eur. J. Pharm. Biopharm.* **1999**, *48*, 1−12.

(9) Bettencourt, A.; Almeida, A. J. Poly(Methyl Methacrylate) Particulate Carriers in Drug Delivery. *J. Microencapsulation* **2012**, *29*, 353−367.

(10) Yu, B.; Cong, H.; Peng, Q.; Gu, C.; Tang, Q.; Xu, X.; Tian, C.; Zhai, F. Current Status and Future Developments in Preparation and Application of Nonspherical Polymer Particles. *Adv. Colloid Interface Sci.* **2018**, *256*, 126−151.

(11) Khoee, S.; Mansouri Bakvand, P. Synthesis of Dual-Responsive Janus Nanovehicle via PNIPAm Modified SPIONs Deposition on Crosslinked Chitosan Microparticles and Decrosslinking Process in the Core. *Eur. Polym. J.* **2019**, *114*, 411−425.

(12) Pourrahimi, A. M.; Pumera, M. Multifunctional and Self-Propelled Spherical Janus Nano/Micromotors: Recent Advances. *Nanoscale* **2018**, *10*, 16398−16415.

(13) Tran, L. T. C.; Lesieur, S.; Faivre, V. Janus Nanoparticles: Materials, Preparation and Recent Advances in Drug Delivery. *Expert Opin. Drug Deliv.* **2014**, *11*, 1061−1074.

(14) Zhang, Q.; Xu, M.; Liu, X.; Zhao, W.; Zong, C.; Yu, Y.; Wang, Q.; Gai, H. Fabrication of Janus Droplets by Evaporation Driven Liquid-Liquid Phase Separation. *Chem. Commun.* **2016**, *52*, 5015−5018.

(15) Chen, S. Q.; He, C.; Li, H. J.; Li, P. Y.; He, W. D. Janus Long-Chain Hyperbranched Copolymers of PSt and POEGMA from a Self-Assembly Mediated Click Reaction. *Polym. Chem.* **2016**, *7*, 2476−2485.

(16) Kang, T.; Li, F.; Baik, S.; Shao, W.; Ling, D.; Hyeon, T. Surface Design of Magnetic Nanoparticles for Stimuli-Responsive Cancer Imaging and Therapy. *Biomaterials* **2017**, *136*, 98−114.

(17) Xue, S.; Xu, X.; Shan, H.; Wang, H.; Yang, J.; Zhou, G. Effects of High-Intensity Ultrasound, High-Pressure Processing, and High-Pressure Homogenization on the Physicochemical and Functional Properties of Myofibrillar Proteins. *Innov. Food Sci. Emerg. Technol.* **2018**, *45*, 354−360.

(18) Venegas-Sánchez, J. A.; Tagaya, M.; Kobayashi, T. Ultrasound Stimulus Inducing Change in Hydrogen Bonded Crosslinking of Aqueous Polyvinyl Alcohols. *Ultrason. Sonochem.* **2014**, *21*, 295−309.

(19) Huo, D.; Kobayashi, T. Sonoresponsive Volume Phase-Transition Behavior of Crosslinked Poly(N-Isopropylacrylamide-Co-Acrylic Acid) Microgel. *Chem. Lett.* **2006**, *35*, 776−777.

(20) Salgarella, A. R.; Zahoranová, A.; Šrámková, P.; Majerčíková, M.; Pavlova, E.; Luxenhofer, R.; Kronek, J.; Lacík, I.; Ricotti, L. Investigation of Drug Release Modulation from Poly(2-Oxazoline) Micelles through Ultrasound. *Sci. Rep.* **2018**, *8*, 9893.

(21) Husseini, G. A.; Myrup, G. D.; Pitt, W. G.; Christensen, D. A.; Rapoport, N. Y. Factors Affecting Acoustically Triggered Release of Drugs from Polymeric Micelles. *J. Controlled Release* **2000**, *69*, 43−52.

(22) Husseini, G. A.; Christensen, D. A.; Rapoport, N. Y.; Pitt, W. G. Ultrasonic Release of Doxorubicin from Pluronic P105 Micelles Stabilized with an Interpenetrating Network of N, N-Diethylacrylamide. *J. Controlled Release* **2002**, *83*, 303−305.

(23) Wang, J.; Pelletier, M.; Zhang, H.; Xia, H.; Zhao, Y. High-Frequency Ultrasound-Responsive Block Copolymer Micelle. *Langmuir* **2009**, *25*, 13201−13205.

(24) Pelletier, M.; Babin, J.; Tremblay, L.; Zhao, Y. Investigation of a New Thermosensitive Block Copolymer Micelle: Hydrolysis, Disruption, and Release. *Langmuir* **2008**, *24*, 12664−12670.

(25) Pei, M.; Jia, X.; Liu, P. Design of Janus-like PMMA-PEG-FA Grafted Fluorescent Carbon Dots and Their Nanoassemblies for Leakage-Free Tumor Theranostic Application. *Mater. Des.* **2018**, *155*, 288−296.

(26) Longenecker, R.; Mu, T.; Hanna, M.; Burke, N. A. D.; Stöver, H. D. H. Thermally Responsive 2-Hydroxyethyl Methacrylate Polymers: Soluble-Insoluble and Soluble-Insoluble-Soluble Transitions. *Macromolecules* **2011**, *44*, 8962−8971.

(27) Higuchi, T. Mechanism of Sustained-Action Medication. Theoretical Analysis of Rate of Release of Solid Drugs Dispersed in Solid Matrices. *J. Pharm. Sci.* **1963**, *52*, 1145−1149.

(28) Korsmeyer, R. W.; Gurny, R.; Doelker, E.; Buri, P.; Peppas, N. A. Mechanisms of Solute Release from Porous Hydrophilic Polymers. *Int. J. Pharm.* **1983**, *15*, 25−35.

(29) Siepmann, J.; Peppas, N. A. Modeling of Drug Release from Delivery Systems Based on Hydroxypropyl Methylcellulose (HPMC). *Adv. Drug Delivery Rev.* **2001**, *48*, 139−157.

(30) Kong, T.; Lin, J.; Ye, L.; Zhang, A.-Y.; Feng, Z.-G. Synthesis of Water Soluble Polyrotaxanes by End-Capping Polypseudo- Rotaxanes of γ-CDs with PHEMA-PPO-PEO-PPO-PHEMA Using ATRP of MPC. *Polym. Chem.* **2015**, *6*, 5832−5837.

(31) Singh, A.; Deshpande, N.; Pramanik, N.; Jhunjhunwala, S.; Rangarajan, A.; Atreya, H. S. Optimized Peptide Based Inhibitors Targeting the Dihydrofolate Reductase Pathway in Cancer. *Sci. Rep.* **2018**, *8*, 3190.

(32) Khoee, S.; Yousefalizadeh, G.; Kavand, A. Preparation of Dual-Targeted Redox-Responsive Nanogels Based on Pegylated Sorbitan

for Targeted and Antitumor Drug Delivery. *Eur. Polym. J.* **2017**, *95*, 448−461.
(33) Lee, W.−. F.; Fu, Y.-T. Effect of Montmorillonite on the Swelling Behavior and Drug-Release Behavior of Nanocomposite Hydrogels. *J. Appl. Polym. Sci.* **2003**, *89*, 3652−3660.
(34) Shukla, V.; Raval, B.; Singh, M. Impact of Newly Synthesized Water Soluble Photoluminescent ZnS-L-Cysteine: Core-Shell Nanoparticles in Defining the in-Situ Opto-Electronic Orbital Model. *Adv. Mater. Lett.* **2016**, *8*, 156−162.
(35) Duan, G.; Zhang, C.; Li, A.; Yang, X.; Lu, L.; Wang, X. Preparation and Characterization of Mesoporous Zirconia Made by Using a Poly (Methyl Methacrylate) Template. *Nanoscale Res. Lett.* **2008**, *3*, 118−122.
(36) Marutani, E.; Yamamoto, S.; Ninjbadgar, T.; Tsujii, Y.; Fukuda, T.; Takano, M. Surface-initiated atom transfer radical polymerization of methyl methacrylate on magnetite nanoparticles. *Polymer* **2004**, *45*, 2231−2235.
(37) Shin, J. M.; Kim, S. H.; Thambi, T.; You, D. G.; Jeon, J.; Lee, J. O.; Chung, B. Y.; Jo, D. G.; Park, J. H. A Hyaluronic Acid-Methotrexate Conjugate for Targeted Therapy of Rheumatoid Arthritis. *Chem. Commun.* **2014**, *50*, 7632−7635.
(38) Rostamizadeh, K.; Manafi, M.; Nosrati, H.; Kheiri Manjili, H.; Danafar, H. Methotrexate-Conjugated MPEG-PCL Copolymers: A Novel Approach for Dual Triggered Drug Delivery. *New J. Chem.* **2018**, *42*, 5937−5945.


https://dx.doi.org/10.1021/acsomega.0c02710
*ACS Omega* 2020, 5, 27119−27132